

Supporting Information

Chhetri et al. 10.1073/pnas.1409321111

SI Text

Framework for Optical Coherence Tomography-Based Measurements of Gold Nanorod Diffusion

Here, we describe a framework for measuring gold nanorod (GNR) diffusion in biological samples via optical coherence tomography (OCT). OCT is a method of low-coherence interferometry in which a broadband light source is used, and the backscattered light from a biological sample is combined with a reference beam (1). In the spectral domain OCT system used in this study, the intensity of the combined beam is measured by a spectrometer (Fig. S1). The resulting spectral interferogram is Fourier transformed to obtain the light-scattering signal from each depth (z) within the sample, where the depth resolution is proportional to the coherence length of the light source (2). To describe stochastic particle motions in this system, we refer to either normalized (g) or unnormalized (G) autocorrelation functions of the light-scattering signals, which are either based on the electric field (first-order), or the intensity (second-order). Because OCT is a heterodyne (mixing) experiment, the heterodyne Siegert relation (1, 2) provides a direct relationship between the second-order autocorrelation $g^{(2)}(\tau)$ of the OCT measurement, and the first-order autocorrelation $g^{(1)}(\tau)$ needed for diffusion measurements:

$$g^{(2)}(\tau) = \text{Re}[g^{(1)}(\tau)].$$

In this way, the real-valued $g^{(1)}(\tau)$ are evaluated directly from the OCT intensity fluctuations.

Now, consider the polarized light scattering from an ensemble of identical particles undergoing Brownian motion that are sufficiently dilute to avoid particle-particle collisions over the timescale of the measurement. When the particles are optically isotropic, the first-order autocorrelation of the scattered field, $G^{(1)}$, is a function of the translational self-diffusion coefficient of the particles, D_T . In the case of optically anisotropic particles, such as GNRs, $G^{(1)}$ is additionally dependent on the rotational self-diffusion, D_R , of the particles (3, 4):

$$G^{(1)}(\tau) \propto \langle \alpha^*(0)\alpha(\tau) \rangle e^{-q^2 D_T \tau},$$

where the polarizability correlation term $\langle \alpha^*(0)\alpha(\tau) \rangle$ depends upon D_R . As polarized light impinges on GNRs, the magnitude and direction of the induced dipole moment fluctuates as the GNRs continually reorient themselves, giving rise to a fluctuating, elliptically polarized, scattered light field. Here, we apply horizontally polarized light (H) onto the sample and detect the horizontal (H) and vertical (V) polarization components of the backscattered field. This field is measured from a spatially resolved volume (the coherence volume) using OCT, in which there is an ensemble of GNRs that give rise to a collective, fluctuating signal. In copolarized detection (HH , i.e., horizontal field applied and horizontal field detected), the field autocorrelation is given by the following:

$$G_{HH}^{(1)}(\tau) \propto \left(\alpha_o^2 + \frac{4}{45} \beta_o^2 e^{-6D_R \tau} \right) e^{-q^2 D_T \tau}.$$

In cross-polarized detection (HV , i.e., horizontal field applied and vertical field detected), the field autocorrelation is given by the following:

$$G_{HV}^{(1)}(\tau) \propto \frac{1}{15} \beta_o^2 e^{-6D_R \tau} e^{-q^2 D_T \tau},$$

where $\alpha_o = (2\alpha_\perp + \alpha_\parallel)/3$ is the mean polarizability, and $\beta_o = (\alpha_\parallel - \alpha_\perp)$ is the anisotropy. Because GNRs are axisymmetric, their polarizability tensor is described by α_\parallel and α_\perp , the components along the long and short axes of the GNRs, respectively. The corresponding normalized first-order autocorrelations, $g^{(1)}$, are then given by the following:

$$\begin{aligned} g_{HH}^{(1)}(\tau) &= \left(\frac{45\alpha_o^2}{45\alpha_o^2 + 4\beta_o^2} \right) e^{-q^2 D_T \tau} + \left(\frac{4\beta_o^2}{45\alpha_o^2 + 4\beta_o^2} \right) e^{-6D_R \tau} e^{-q^2 D_T \tau} \\ g_{HV}^{(1)}(\tau) &= e^{-6D_R \tau} e^{-q^2 D_T \tau}. \end{aligned} \quad [\text{S1}]$$

Importantly, at the longitudinal surface plasmon resonance of the GNRs, $\alpha_\parallel \gg \alpha_\perp$; using previously reported computational methods (3), we estimate that $\alpha_\parallel/\alpha_\perp \sim 1,600$ for the GNRs in this study. Thus, the mean polarizability α_o and optical anisotropy β_o of GNRs can be approximated as $\alpha_\parallel/3$ and α_\parallel , respectively. One important consequence of the large optical anisotropy of GNRs is that it gives rise to large contrast in cross-polarized (HV) images, which allows GNRs to be distinguished within biological tissues which are only weakly anisotropic. The other consequence is that the normalized first-order autocorrelations simplify to the following:

$$\begin{aligned} g_{HH}^{(1)}(\tau) &= \left(\frac{5}{9} \right) e^{-q^2 D_T \tau} + \left(\frac{4}{9} \right) e^{-6D_R \tau} e^{-q^2 D_T \tau} \\ g_{HV}^{(1)}(\tau) &= e^{-6D_R \tau} e^{-q^2 D_T \tau}. \end{aligned} \quad [\text{S2}]$$

A linear combination of these autocorrelations isolates the D_T term, which is known as the isotropic autocorrelation, $g_{ISO}^{(1)}$:

$$g_{ISO}^{(1)}(\tau) = \left(\frac{9}{5} \right) g_{HH}^{(1)}(\tau) - \left(\frac{4}{5} \right) g_{HV}^{(1)}(\tau) = e^{-q^2 D_T \tau}. \quad [\text{S3}]$$

Using this expression, we obtain the D_T of an ensemble of GNRs from measurements of $g_{HH}^{(1)}$ and $g_{HV}^{(1)}$. Also, because the GNRs in this study are small compared with the wavelength ($L < \lambda$), the $1/e$ decay time associated with D_T is much longer than D_R [i.e., $6D_R/q^2 D_T$ varies with $(\lambda/L)^2$ and ~ 9 in this study]. Thus, the D_R of an ensemble of GNRs can be obtained using the following approximation:

$$g_{HV}^{(1)}(\tau) \approx e^{-6D_R \tau}. \quad [\text{S4}]$$

Although the GNRs in our study are not perfectly identical, we find that they are sufficiently monodisperse such that the $g_{HV}^{(1)}$ and $g_{ISO}^{(1)}$ are well described by single-exponential decays, which can be thought of as ensemble-averaged measurements.

Importantly, for GNRs, the approximate $1/e$ decay time observed for $g_{HH}^{(1)}(\tau)$ (Eq. S2) is weighted by both D_R and D_T and does not fit a single exponential. In comparison, τ_{HV} (Eq. S4) is dominated by D_R and is therefore significantly shorter. This is in contrast to light-scattering signals from cells, which are described more generally by Eq. S1 with additional fluctuations due to cellular motility. If we consider that cells are not plasmon resonant, cellular features (refractive index heterogeneities) on the order of $L \sim \lambda$ tend to dominate the light-scattering signal. In this

case, the decay mode anisotropy disappears because both τ_{HH} and τ_{HV} depend strongly on D_T . Also, the decay rates from cells

are slower than those of GNRs owing to the larger hydrodynamic sizes of the scatterers.

1. Huang D, et al. (1991) Optical coherence tomography. *Science* 254(5035):1178–1181.
2. Fercher AF, Hitzenberger CK, Kamp G, El-Zaiat SY (1995) Measurement of intraocular distances by backscattering spectral interferometry. *Opt Commun* 117(1-2):43–48.
3. Berne BJ, Pecora R (1976) *Dynamic Light Scattering* (Dover Publications, New York).
4. Johnson CS, Jr, Gabriel DA (1981) *Laser Light Scattering* (Dover Publications, New York).

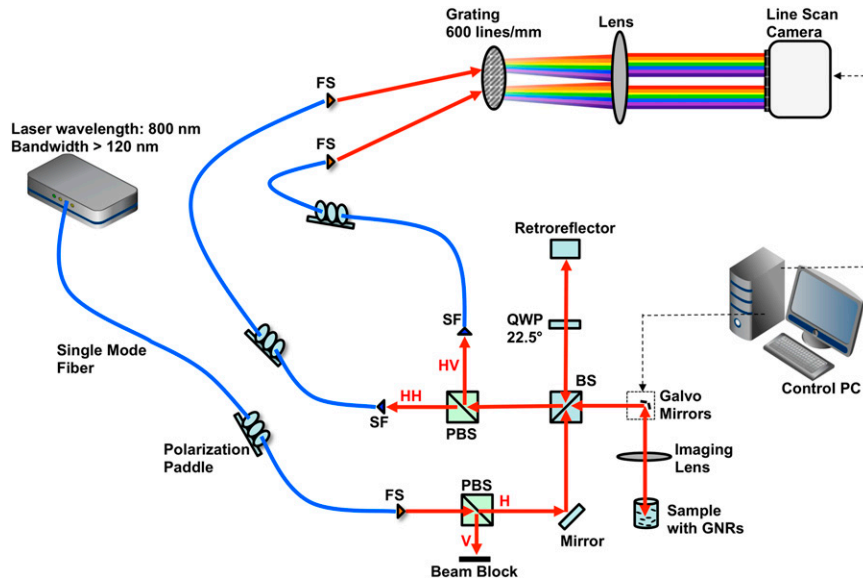


Fig. S1. Schematic of the custom OCT system. Light from a Ti:sapphire laser is guided to a free-space Michelson interferometer, and the polarization-dependent interferograms are detected by a free-space spectrometer. BS, 50–50 nonpolarizing beam splitter; FS, fiber to free-space coupler; HH, copolarized component; HV, cross-polarized component; PBS, 50–50 polarizing beam splitter; QWP, quarter wave plate; SF, free-space to fiber coupler.

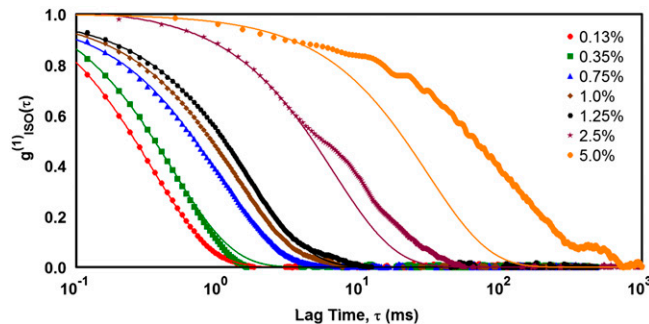


Fig. S2. Inverse exponential fitting to isotropic temporal autocorrelations [$g_{ISO}^{(1)}(\tau)$] of GNRs in 1-MDa PEO at varying concentrations. In the weakly constrained regime [PEO concentration $\leq 1.25\%$ (wt/wt)], $g_{ISO}^{(1)}(\tau)$ is well described by an inverse exponential, and thus the diffusion rate of GNRs is well defined within the timescale of the measurement. At higher concentrations, the viscoelasticity of the PEO causes significant deviation of $g_{ISO}^{(1)}(\tau)$ from a single exponential. [Fit lines for 2.5% (wt/wt) and 5.0% (wt/wt) are for illustrative purposes only and were performed for $g_{ISO}^{(1)}(\tau) > 0.6$ and 0.88, respectively. All other lines were fitted for $g_{ISO}^{(1)}(\tau) > 1/e$ as in *Materials and Methods*.]

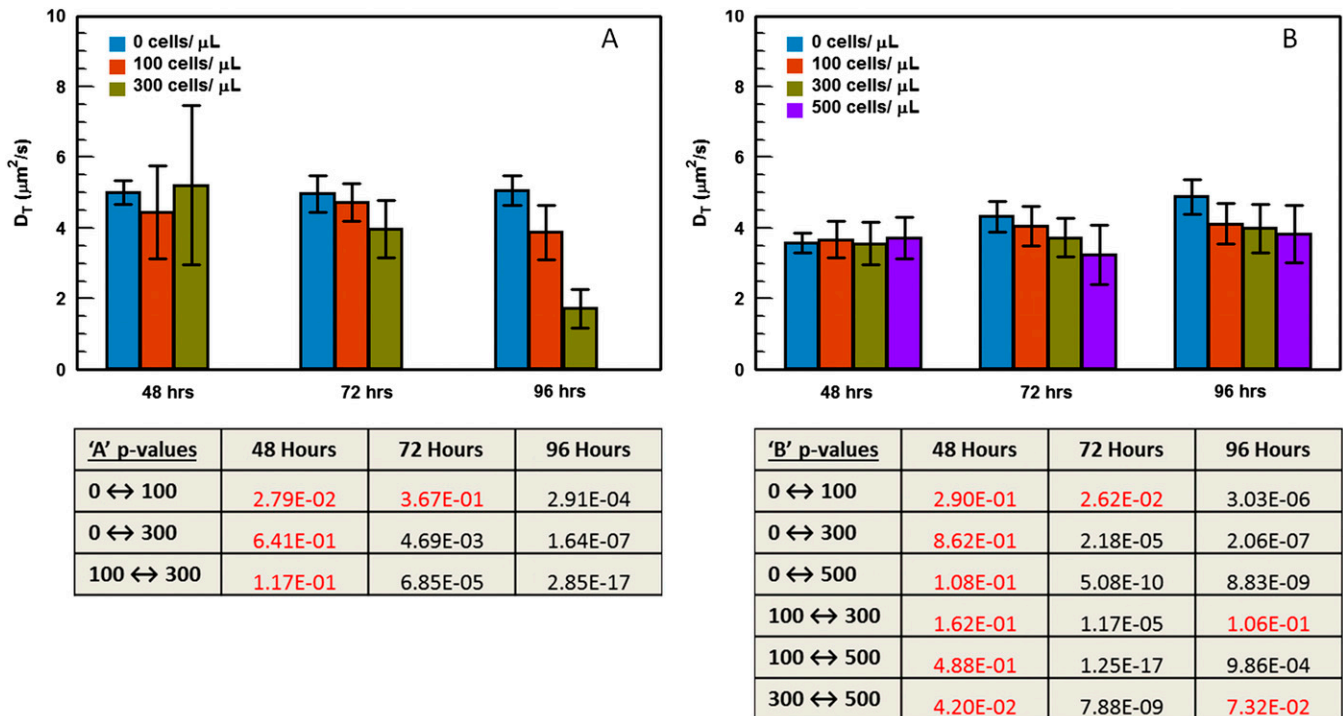


Fig. S3. Diffusion rate of GNRs in 3D cultures for increasing fibroblast density and incubation time. Two additional trials of experiments with fibroblasts were conducted to demonstrate reproducibility of the trend reported in Fig. 2D. (A) Comparison of three seed densities over three separate incubation times (control, $n = 12$; all other, $n = 24\text{--}36$; average and SD), with the decrease in diffusion of GNRs for higher cell concentrations becoming more significant as the incubation time increases. (B) Comparison of four seed densities for the three incubation times (control, $n = 12$; all other, $n = 96\text{--}156$; average and SD), with decreasing diffusion rates of GNRs for higher cell concentrations evident at the longer two incubation times, 72 and 96 h. P values for D_T measurements comparing different cell seed densities at each incubation time are given in tables corresponding to the fibroblast data reported in each panel.

Table S1. P values for D_T measurements comparing different collagen concentrations, corresponding to the data reported in Fig. 2B

Comparison	P value
CM ↔ 1 mg/mL	7.08E-03
CM ↔ 2 mg/mL	2.09E-05
CM ↔ 3 mg/mL	1.63E-06
1 mg/mL ↔ 2 mg/mL	1.07E-03
1 mg/mL ↔ 3 mg/mL	6.21E-05
2 mg/mL ↔ 3 mg/mL	4.18E-02

CM represents cell media control. Statistically significant values are displayed in black, and insignificant value is in red.

Table S2. P values for D_T measurements comparing different cell seed densities at each incubation time, corresponding to the fibroblast data reported in Fig. 2D

Comparison	48 h	72 h	96 h
0 ↔ 100	7.90E-03	3.14E-04	1.00E-05
0 ↔ 300	4.66E-06	7.57E-09	2.57E-07
0 ↔ 500	1.75E-07	8.36E-07	1.45E-06
100 ↔ 300	9.59E-07	1.36E-21	8.74E-19
100 ↔ 500	4.09E-06	1.95E-07	1.64E-04
300 ↔ 500	1.39E-01	1.07E-09	3.60E-06

Statistically significant values are displayed in black, and insignificant value is in red.